Wagner, F., Bergmann, P., Rücker, C., Wiese, B., Labitzke, T., Schmidt-Hattenberger, C., Maurer, H. (2015): Impact and mitigation of borehole related effects in permanent crosshole resistivity imaging: An example from the Ketzin CO2 storage site. - *Journal of Applied Geophysics*, *123*, p. 102-111.

DOI: http://doi.org/10.1016/j.jappgeo.2015.10.005

Journal of Applied Geophysics 123 (2015) 102–111

Contents lists available at ScienceDirect

Journal of Applied Geophysics

journal homepage: www.elsevier.com/locate/jappgeo

Impact and mitigation of borehole related effects in permanent crosshole resistivity imaging: An example from the Ketzin CO_2 storage site

Florian M. Wagner [a,b,*], Peter Bergmann [a,c], Carsten Rücker [d], Bernd Wiese [a], Tim Labitzke [a], Cornelia Schmidt-Hattenberger [a], Hansruedi Maurer [b]

[a] GFZ German Research Centre for Geosciences, Centre for Geological Storage, Potsdam, Germany
[b] ETH Zurich, Institute of Geophysics, Zurich, Switzerland
[c] Sintef Petroleum Research, Trondheim, Norway
[d] Berlin University of Technology, Department of Applied Geophysics, Berlin, Germany

ARTICLE INFO

Article history:
Received 13 July 2015
Received in revised form 29 September 2015
Accepted 6 October 2015
Available online 9 October 2015

Keywords:
Electrical resistivity tomography (ERT)
Permanent electrodes
Borehole effects
CO_2 injection monitoring
Ketzin

ABSTRACT

Geoelectrical methods are particularly suited for CO_2 injection monitoring due to their high sensitivity to fluid displacement processes in porous rock formations. The use of borehole electrodes is favorable for deep storage horizons. Yet data acquisition based on permanently installed borehole electrodes can be challenged by the finite extent of the electrodes, unintended borehole deviation and complex borehole completion. Such conditions can lead to systematic errors in the electrical data sets, distortions of tomograms, and ultimately misinterpretations. We systematically analyze the effects of different borehole related error sources on tomographic inversion results and present respective methods for mitigation. Specifically, we incorporate the finite extent of the ring electrodes and the borehole completion into the electrical finite-element models and discuss the opportunity to infer borehole deviations solely based on geoelectrical data by means of a coupled inversion. While the finite extent of ring electrodes can be neglected if the electrode spacing is sufficiently large (>5 m), different borehole completion materials used to fill the well annulus can cause potentially strong resistivity contrasts between the borehole completion and the rock formation, i.e., close to the electrodes. Resulting inversion artifacts are generally less severe when the borehole completion is more resistive compared to the surrounding rock. It is also shown that 2.5D inversion approaches are not adequate for imaging injection experiments in the presence of borehole completion. Unintended borehole deviation can result in geometric errors. Especially, vertical electrode shifts cause strong and localized inversion artifacts. Coupled inverse schemes potentially provide the opportunity to infer electrode shifts solely based on geoelectrical data provided the availability of high quality measurements (<5% data error). After discussing the effects of the different borehole related error sources, the mitigation methods are validated using synthetic data sets. Subsequently, relevant methods are applied to a field data set from the Ketzin CO_2 storage site, Germany, where crosshole electrical resistivity imaging is used for CO_2 migration monitoring. The mitigation methods presented can improve estimates of the subsurface resistivity distribution, which, in our particular example, is an essential basis for the quantification of CO_2 saturation from time-lapse geoelectrical measurements.

1. Introduction

Electrical resistivity tomography (ERT) is well suited to monitor dynamic flow and transport processes in the subsurface due to its high sensitivity with regard to the presence and composition of pore fluids. The method is well established in near-surface geophysics (e.g. Binley and Kemna, 2005; Loke et al., 2013). More recently, ERT has received consideration as a tool for subsurface monitoring at larger depths of up to ≈3 km by means of permanently installed borehole electrodes. Successful deep electrode installations include the CO_2 storage sites at Cranfield, Mississippi, US (Carrigan et al., 2013; Yang et al., 2014) and Ketzin, Germany (Bergmann et al., 2012; Schmidt-Hattenberger et al., 2013). A further installation is planned at the Hontomín site in Spain (Vilamajó et al., 2013). ERT has also been used to monitor the development of oil extraction chambers during steam assisted gravity drainage (SAGD) in the Athabasca tar sand region in Canada (Tøndel et al., 2014) and is considered as a surveillance tool for gas-based energy storage (Hagrey et al., 2014).

In addition to the obvious practical challenges associated with the installation of permanent borehole electrodes at typical reservoir depths of a few kilometers, the borehole itself represents a delicate environment for geoelectrical data acquisition and requires particular

* Corresponding author at: GFZ German Research Centre for Geosciences, Centre for Geological Storage, Potsdam, Germany.
E-mail address: florian.wagner@gfz-potsdam.de (F.M. Wagner).

http://dx.doi.org/10.1016/j.jappgeo.2015.10.005
0926-9851/

attention. Problems can arise due to (i) ring-shaped electrodes having variable electrical contact to the rock formation, (ii) geometric errors as a consequence of borehole deviations, and (iii) strong resistivity contrasts in the proximity of the electrodes due to various materials being used for borehole completion. In consequence, tomographic inversions can be significantly deteriorated, which may result in spurious ERT images and misinterpretations (Wilkinson et al., 2008; Doetsch et al., 2010). This paper presents the first study dedicated to borehole related errors associated with deep permanent electrode installations. Building on significant advances made in near-surface studies, we investigate the implications of different borehole related effects and present means of mitigation with an application to ERT data from the Ketzin CO_2 storage site, Germany.

2. Field site description

The Ketzin site is located approximately 40 km west of Berlin, Germany, geologically located in the Roscow–Ketzin double anticline within the Northeast German Basin. Between June 2008 and August 2013, 67 kt of CO_2 have been stored in the upper part of the Stuttgart formation, a sandstone of the Upper Triassic, at approximately 635 m depth (Kühn et al., 2015). Fig. 1 contains lithological profiles of the injection well (Ktzi201) and the first two observations wells (Ktzi200 and Ktzi202). Within the Stuttgart formation, sandy channel-facies rocks of good reservoir quality alternate with muddy flood-plain-facies rocks of poor reservoir quality. The overlying Weser formation primarily consists of clayey siltstones, carbonates and evaporites with suitable sealing properties (Förster et al., 2006). A detailed geological characterization of the site can be found in Norden and Frykman (2013). The Ketzin project has a strong focus on developing and assessing benefits and limitations of different techniques for CO_2 migration monitoring (Köhler et al., 2013). An overview of the applied methods including a list of references to the conducted field studies is provided by Martens et al. (2014).

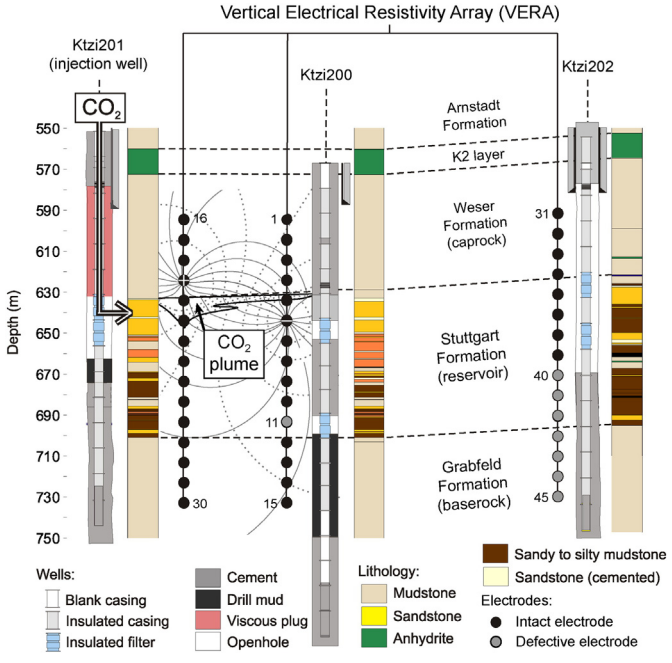

Fig. 1. Schematic illustration of lithology, borehole completion and permanent electrode installation at the Ketzin site modified after Bergmann et al. (2012). Lithological information is based on Förster et al. (2006).

2.1. Permanent electrode installation

As part of the multi-method monitoring program, a permanent vertical resistivity array (VERA) has been deployed in the injection well and the first two observation wells at the Ketzin site in order to monitor the electrical subsurface properties at a high temporal resolution (Schmidt-Hattenberger et al., 2012). Fig. 1 shows a schematic of the electrode installation together with lithological information and details on the well completion.

VERA consists of 45 ring-shaped stainless steel electrodes mounted on the borehole casing. The casings were coated with an electrically insulating membrane in the depth interval hosting the electrodes. A photo of an electrode is presented in Fig. 3a. Multi-conductor cables protected by centralizers were used to connect the individual electrodes to the acquisition system at the surface. Since the beginning of CO_2 injection in 2008, ERT measurements have been repeated weekly. Measured data sets consist of bipole–bipole configurations, where the two electrodes of a bipole are either situated in one borehole (AB-MN) or split across different boreholes (AM-BN). This was supplemented by limited number of inhole measurements as discussed in detail by Schmidt-Hattenberger et al. (2011). During the early stage of injection operation, connections to the seven lowermost electrodes in well Ktzi202 (starting at the onset of cementation) were lost, most likely as a consequence of cable damages resulting from the installation procedure. Since the scarcity of intact electrodes in the second observation well challenges 3D imaging, we focus our investigation on the imaging plane between the injection well Ktzi201 and the first observation well Ktzi200, where only electrode #11 is known to be defective (Fig. 1).

2.2. Borehole completion

In order to maintain integrity of the boreholes after the drilling procedure, the well annuli were backfilled with cement and a viscous plug consisting of Xanthan gum. In addition, residues of drill mud remained in Ktzi200 and Ktzi201 as illustrated in Fig. 1. To avoid potential damage of the cables as a consequence of subsequent perforation, a staged cementation process was realized using a swellable packer, which allowed for completion of open hole intervals with filter screens in all three wells (Prevedel et al., 2008).

2.3. Borehole deviation

Fig. 2 shows the borehole deviation of the three Ketzin wells relative to the respective wellheads modified after (Götz, 2013). Differences between measured and true vertical depths of the wells are within the centimeter range, and have also been found to be a negligible issue in previous seismic crosshole tomography studies (Götz, 2013). Along the casings, vertical deviations from the nominal electrode spacing of 10 m occur due to technical reasons. More specifically, some electrode positions were shifted to avoid electrodes being placed on the filter screens. Nominal electrode positions assume an equidistant electrode spacing of 10 m on straight boreholes and were used in previous studies (e.g. Kiessling et al., 2010; Bergmann et al., 2012; Schmidt-Hattenberger et al., 2014).

3. Effects of finite electrode size

In electrical forward models, electrodes are commonly represented as point sources located on the nodes of a finite-difference or finite-element discretization. However, Rücker and Günther (2011) report that the shape and spatial extent of an electrode can have a considerable influence on resistivity measurements, especially for circular electrode geometries and for measurements at laboratory scale. To assess the relevance of the finite electrode size for the Ketzin case, the metal rings, constituting the electrodes with a diameter of 15 cm and a height of 10 cm, are explicitly discretized in the finite-element mesh. In addition,

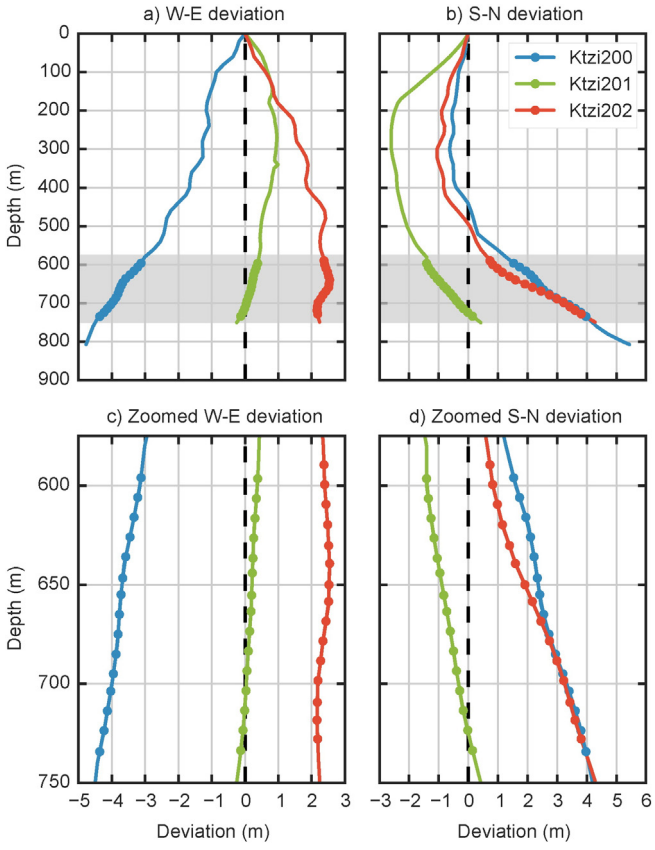

Fig. 2. Measured borehole deviation in S–N (a) and W–E directions (b) relative to the wellhead modified after (Götz, 2013). The gray shaded areas correspond to panels (c) and (d), which show vertically enlarged sections of the depth interval containing the electrodes. Dots mark electrode positions.

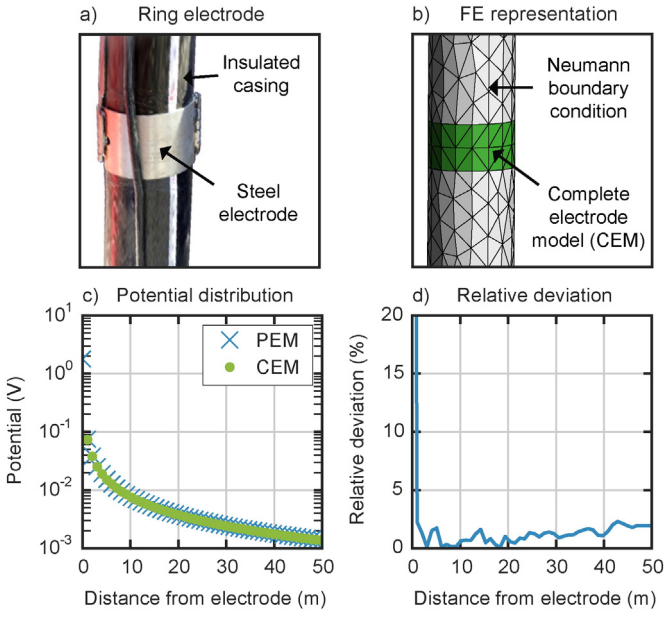

Fig. 3. (a) Ring-shaped stainless steel electrode mounted on the electrically insulated borehole casing. (b) Corresponding finite-element discretization. (c) Decay of electrical potential away from the source. Blue crosses and green dots correspond to the Point Electrode Model (PEM) and the Complete Electrode Model (CEM), respectively. (d) Relative deviation of the potential decay between PEM and CEM. (For interpretation of the references to color in this figure legend, the reader is referred to the web version of this article.)

a Neumann boundary condition is applied to the representation of the electrically insulated casing as illustrated in Fig. 3b.

Based on this discretization, the complete electrode model (CEM) following Rücker and Günther (2011) and a conventional point electrode model (PEM) are compared in a homogeneous space with a resistivity of 1 Ωm. To ensure numerical accuracy, the meshes were refined until the deviation of the PEM simulation from a corresponding analytical solution was less than 0.2%. Fig. 3c shows the decay of the electrical potential with increasing radial distance to a single source for the PEM (blue crosses) and the CEM (green dots). Fig. 3d shows the corresponding relative deviation. For the source singularity ($x = 0$) associated to the PEM, a significant error is observed. For increasing distance, however, relative deviations are found to be very low, i.e. the relative deviation decreases to values smaller than 2% within the first meter away from the source.

Fig. 4 shows the electrode effect, i.e. the relative deviation of a resistance measurement modeled with the PEM and the CEM for a conventional 5.5 inch casing, as a function of decreasing electrode spacing for different measurement configurations using two, three, and four electrodes.

The magnitude of the electrode effect shows exponential growth with decreasing electrode spacing, and exhibits only marginal differences between the types of measurement configurations. For an electrode spacing of 10 m as present at the Ketzin site, the relative deviation of a dipole–dipole measurement with four adjacent electrodes is 2.3%. Schmidt-Hattenberger et al. (2014) report that at Ketzin, the median of the relative deviation between measurements and their complementary reciprocals, hereinafter referred to as median reciprocal error, ranges between 5% and 10% over the whole injection period. With regard to this general noise level, we consider a point approximation of the electrodes to be an adequate representation. For smaller electrode spacings, however, the electrode effect may be comparable to or even exceed the noise level. In such cases, we recommend to account for the finite spatial extent of the electrodes as well as the geometrical disturbance caused by the insulated borehole casings by using the complete electrode model.

4. Effects of borehole completion

In deep cased boreholes, the space between the borehole casings and the rock formation is usually backfilled to avoid hydraulic conduits along the well annuli. At the Ketzin site, some depth intervals of the well annulus are not cemented, others are backfilled with a viscous Xanthan plug or drill mud as shown in Fig. 1. This diversity of materials used for filling of the well annuli, and in particular the presence of uncemented parts, are known to have an impact on electrical surface-downhole measurements and pulsed neutron-gamma logs at the Ketzin site

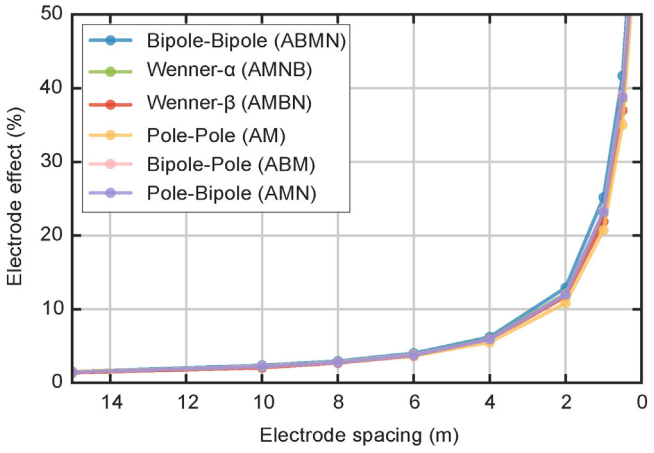

Fig. 4. Electrode effect as a function of electrode spacing for different measurement configurations. A and B mark the current electrodes and M and N mark the potential electrodes.

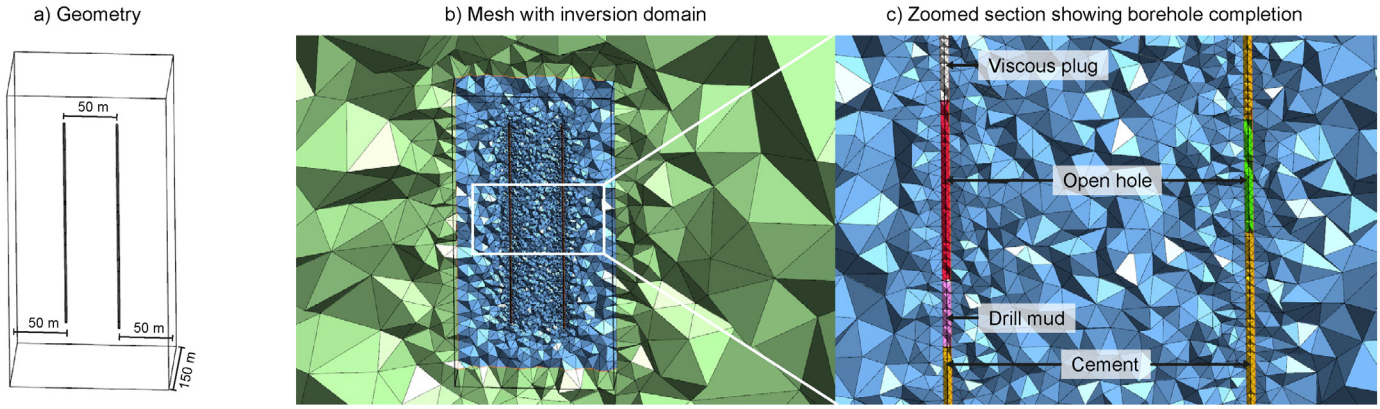

Fig. 5. a) Geometry of the inversion domain including the boreholes. b) 3D finite-element discretization. Blue elements correspond to the inversion domain. Green elements correspond to the background region additionally used to solve the forward problem. c) Zoomed section showing the explicitly discretized borehole regions corresponding to the completion types in Fig. 1. (For interpretation of the references to color in this figure legend, the reader is referred to the web version of this article.)

(Bergmann et al., 2012; Baumann et al., 2014). In near-surface ERT, the resistivity contrast between the borehole filling fluid and the rock formation is also known to be a source of systematic data errors that can produce spurious features in the inversion images (Osiensky et al., 2004; Nimmer et al., 2008; Doetsch et al., 2010). Nimmer et al. (2008) emphasize that a 2.5D inversion approach, i.e. a two-dimensional inversion which implies expansion of resistivities in the direction perpendicular to the imaging plane, can yield artifacts when anomalous off plane features are present. Analogously, it is not valid to assume that borehole related features extend infinitely into the direction perpendicular to the imaging plane. We therefore additionally compare the tomographic reconstruction capabilities of 2.5D and 3D inversions here in the context of borehole completion.

4.1. Impacts

To model the effect of the borehole completion for the Ketzin case, we explicitly discretized the different completion regions (as schematically shown in Fig. 1) in an unstructured tetrahedral mesh. The finite-element discretization is illustrated in Fig. 5.

The boreholes were represented by two cylinders consisting of vertically arranged segments according to the completion materials. While the resistivity of the cemented parts, the viscous plug, as well as the drill mud may be relatively constant over time, the open hole intervals (white parts in Fig. 1) can be saturated with conductive brine, resistive supercritical CO_2, or a mixture of both and can consequently exhibit rapid resistivity changes. To assess the influence of the borehole completion and in particular the open hole parts, the response for a three layer baseline model is simulated for two different scenarios representing brine and CO_2 prevailing conditions assuming resistivity values listed in Table 1.

To ensure accuracy during 3D forward modeling, we use a refined version of the mesh shown in Fig. 5 obtained from bisection of each edge. The green cell region in Fig. 5b is only used during forward modeling and extends to the surface and to 5 km in x, y and z directions. All data sets consist of 1025 four-point configurations contaminated with Gaussian noise of 3% and a voltage error of 50 μV.

Fig. 6a shows the true model and Fig. 6b and c shows the inversion results for the conductive case using a 2.5D and a 3D inversion approach, respectively. The 2.5D and 3D inversion meshes have 3500 and 120,000 parameter cells, respectively. Note that for a comparative visualization, all 2.5D and 3D inversion results are interpolated to the same two-dimensional mesh using a nearest-neighbor approach.

For the conductive case, both inversion results contain significant artifacts and fail to sufficiently recover the true formation resistivities. The artifacts are more pronounced when using a 2.5D inversion (Fig. 6b). For the resistive case, the inversion results in 2.5D and 3D (Fig. 6e and f) show no significant artifacts and are closer to the true model, although the 2.5D inversion overestimates and underestimates the resistivities of the caprock and baserock layers by up to about 35% and 25%, respectively.

Table 1
Resistivity values assigned to different borehole completion regions for generation of synthetic data.

Scenario	Cement	Viscous plug	Drill mud	Open hole
#1 (brine prevailing)	15 Ωm	10 Ωm	1 Ωm	0.01 Ωm
#2 (CO_2 prevailing)	15 Ωm	10 Ωm	1 Ωm	1000 Ωm

4.2. Mitigation

Doetsch et al. (2010) found that a full 3D representation the boreholes using unstructured finite-element meshes can allow for more accurate forward modeling and improved inversion results in 3D ERT. We adopt a similar approach by using the mesh shown in Fig. 5 for the inversion. Thereby, the smoothness constraint is locally decreased at the boundary between the borehole completion and the formation by 75%. This allows, but does not force, the parameter distribution to behave discontinuously across these predefined boundaries. In addition, the regularization within the borehole completion regions was increased by a factor of five in order to compensate for the 70,000 additional parameters resulting from mesh refinements within the borehole completion region. Hereinafter, we refer to this inversion as borehole constrained inversion.

4.2.1. Synthetic example

We have applied the borehole constrained inversion to the synthetic scenario presented in Fig. 6. Fig. 6d and g shows the results of a borehole constrained inversion when the open hole parts are more conductive and more resistive with respect to the rock formation, respectively. In both cases, the constrained inversion provides better reconstructions of the true underlying models compared to the conventional 2.5D and 3D inversions.

A quantitative analysis is presented in Fig. 7, where the true resistivity values of the two scenarios are plotted against the mean of the respective estimates obtained from the borehole constrained inversion. Although the borehole constrained inversion fails to accurately recover the resistivity values of the borehole completion in few cases, i.e. the value of the CO_2 filled open hole parts (gray square) is underestimated by two orders of magnitude, the estimated resistivities of the three layer model (blue, green, and red) generally correspond well to the true values.

The synthetic experiment shows that the uncemented parts can introduce strong imaging artifacts under brine prevailing conditions

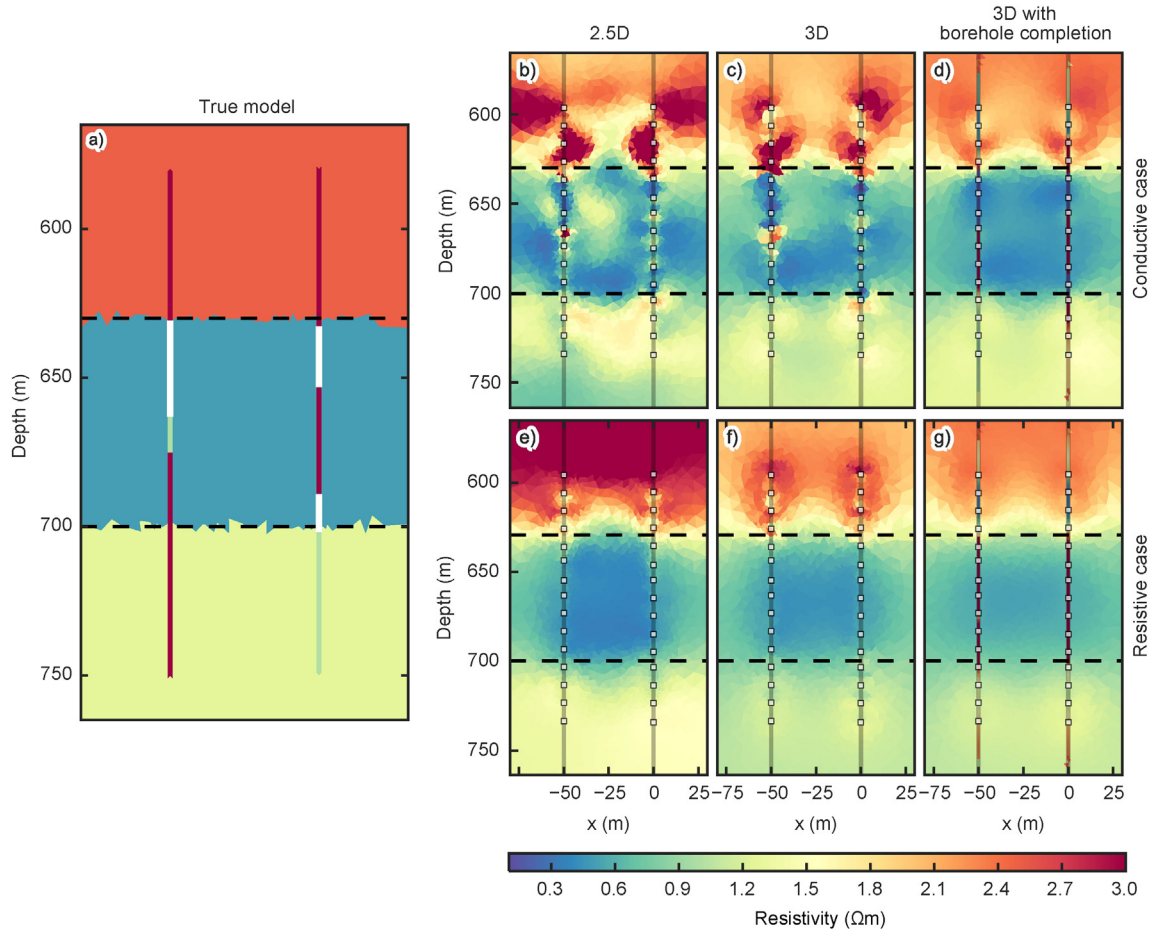

Fig. 6. (a) Three layer model where the open hole parts (white intervals) are assumed to be either brine saturated and highly conductive (scenario #1 in Table 1) or CO_2 saturated and resistive (scenario #2 in Table 1). (b–d) Inversion results in 2.5D, 3D, and 3D with an explicit discretization and decoupling of the borehole completion for the conductive case. (e–g) Inversion results in 2.5D, 3D, and 3D with an explicit discretization and decoupling of the borehole completion for the resistive case layer boundaries are marked by the black dashed lines. Note that the color bar is clipped at 3 Ωm. (For interpretation of the references to color in this figure legend, the reader is referred to the web version of this article.)

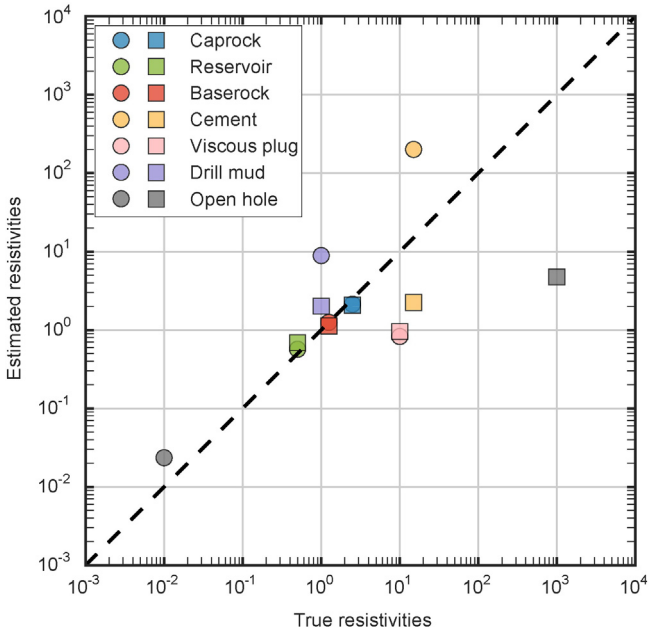

Fig. 7. True resistivity values plotted against their respective mean estimates provided by the borehole constrained inversion. Circles and squares correspond to the conductive and resistive scenario, respectively.

when using conventional 2.5D and 3D inversions, while the situation is generally less severe for a CO_2 prevailing scenario, i.e. more resistive borehole completions. In both cases, the best inversion results are obtained when the regularization strength is loosened between the borehole completion and the rock formation. Although the borehole constrained inversion fails to accurately recover the absolute values of the strong small-scale resistivity anomalies related to the borehole completion, the true formation resistivities are accurately imaged. This also suggests that a detailed analysis of the electrical properties of the borehole completion materials is not a necessity for tomographic imaging.

4.2.2. Ketzin example

We additionally apply the explicit borehole completion discretization to the Ketzin baseline data set from June 21 in 2008 prior to CO_2 injection. The inversion results using a conventional 2.5D, a conventional 3D, and a borehole constrained inversion are shown in Fig. 8. The known lithological boundaries of the Stuttgart formation are marked by the black dashed lines. Data weighting is performed in analogy to the synthetic example by an error model assuming a base error level of 3% and a voltage error of 50 μV following the approach of Friedel (2003).

The 2.5D inversion (Fig. 8a) shows a low resistive background model with some near-electrode anomalies and high resistive features in the corners of the imaging plane. These are significantly reduced by a 3D inversion (Fig. 8b). The strong resistive artifacts are further reduced by the

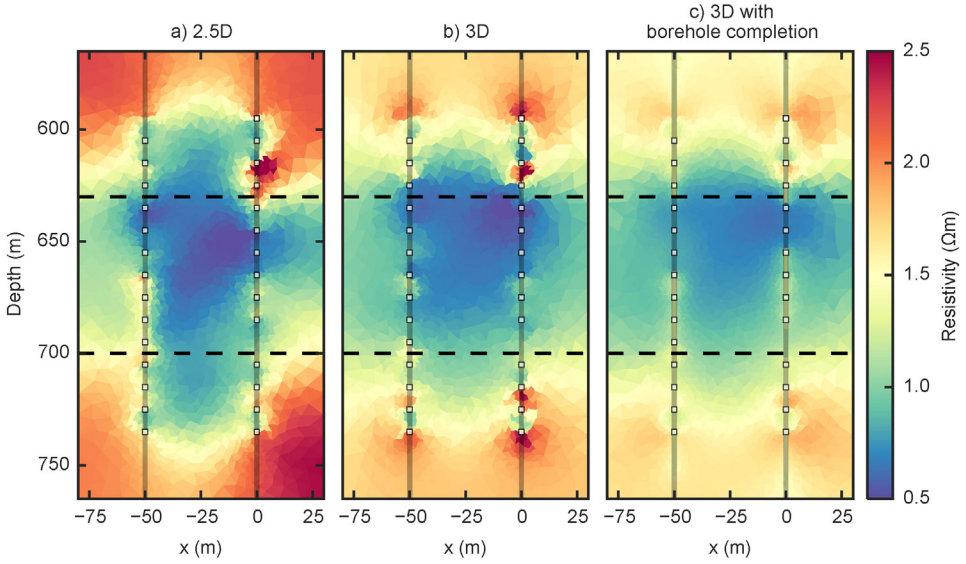

Fig. 8. Inversion of the Ketzin baseline data set from June 21, 2008. (a) 2.5D inversion, (b) 3D inversion, and (c) 3D inversion with an explicit discretization of the borehole completion.

borehole constrained inversion (Fig. 8c), which also leads to a better delineation of the known lithological boundaries.

We attribute this to the fact that localized resistivity anomalies caused by the borehole completion do not extend infinitely into the direction perpendicular to the imaging plane and thereby violate the fundamental assumption made in 2.5D inversions (e.g. Nimmer et al., 2008). It is noteworthy that all presented inversion results are able to explain the data in consideration of the underlying error model. In other words, borehole completion related resistivity structures are entirely compensated by imaging artifacts within conventional inversions, which challenges image appraisal based on data fits.

Fig. 9 shows the resistivity ratio between the baseline model and four consecutive timesteps in the early injection phase for the different inversion approaches. While the conventional 2.5D inversion (Fig. 9a–d) contains high resistive features along the left borehole (Ktzi201), the resistivity increase is thinner and more localized at the point of injection for the conventional 3D inversion (Fig. 9e–h). Again, the significant improvement is visible when moving from 2.5D to 3D, while a decoupling of the borehole completion regions (Fig. 9i–l) does not lead to a notable change. The lowermost row (Fig. 9m–p) shows depth slices through the resistive anomaly at $y = 650$ m of the borehole constrained inversion. Depth slices of the conventional 3D inversion look similar and are not shown here. The depth slices reveal that the 3D inversion approach is able to develop a circular resistive anomaly around the injection well, which is not possible in 2.5D inversions.

5. Effects of borehole deviation

Geometric errors resulting from deviations of the borehole trajectories are a common concern in borehole based geophysical surveying, particularly for travel time tomography using seismic (Maurer, 1996) and electromagnetic waves (Maurer and Musil, 2004). Unintentional and unknown borehole deviations can also severely deteriorate electrical resistivity tomograms as demonstrated by Oldenborger et al. (2005), Wilkinson et al. (2008), and Yi et al. (2009).

5.1. Impacts

To evaluate the impacts of borehole deviation for the Ketzin case specifically, synthetic experiments with different electrode positions during forward modeling and inversion were performed (Fig. 10). In Fig. 10a–e, black dots denote electrode positions used to generate the synthetic data sets, whereas blue crosses mark the positions assumed during tomographic inversion. Borehole deviations assumed during forward modeling are based on the measured borehole deviations at the Ketzin site (e.g. Götz, 2013) and plotted in Fig. 2. All synthetic data sets were calculated using the analytical solution for a homogeneous space, and subsequently contaminated with Gaussian noise of 3% and a voltage error of 50 μV. The corresponding inversion results are shown in the lower row (Fig. 10f–j) and plotted as the relative deviation from the true homogeneous model.

In situations where identical electrode positions have been used for forward modeling and inversion (Fig. 10a), the deviations from the true model are found to be within the range of the data errors. If the same data set is inverted assuming strictly vertical borehole trajectories and an equidistant electrode spacing of 10 m (Fig. 10b), relative deviations from the true model are significantly larger, reaching errors of 80% (Fig. 10g). To investigate the impact of borehole deviation with respect to the different spatial directions, synthetic data sets were calculated considering deviations only in x (Fig. 10c), y (Fig. 10d), and z directions (Fig. 10e). The westerly deviation of Ktzi200 by about 3.5 m (Fig. 10c) results in shorter distances to the electrodes in Ktzi201, which in turn results in a systematic underestimation of the subsurface resistivity between the wells by about 21%. This is compensated by notably overestimated resistivities outside the imaging region surrounded by the electrodes as evident in Fig. 10h. The effect of the borehole deviation in y direction is shown in Fig. 10i. The tomogram is very similar to the inversion result with the true electrode positions (Fig. 10f) indicating that the NS deviations, i.e. perpendicular to the imaging plane, have a negligible effect on the tomographic image. Deviations in z direction have a strong influence on the inverted resistivity close to the shifted electrodes and result in a strong and non-uniform overestimation between the wells (Fig. 10j). Ultimately, the impact of the three-dimensional borehole deviation (Fig. 10g) is mainly constituted of horizontal and vertical shifts within the imaging plane (i.e., a combination of Fig. 10h and j), whereby the overestimation between the wells resulting from vertical shifts is partly counterbalanced by the in-plane shifts (Fig. 10h).

5.2. Mitigation

When the borehole deviation cannot be accurately measured, an alternative approach may be the estimation of borehole deviation based on geoelectrical data. Following advancements in medical imaging (e.g. Soleimani et al., 2006), it has recently been proposed to invert for electrode positions and resistivity distribution simultaneously in the

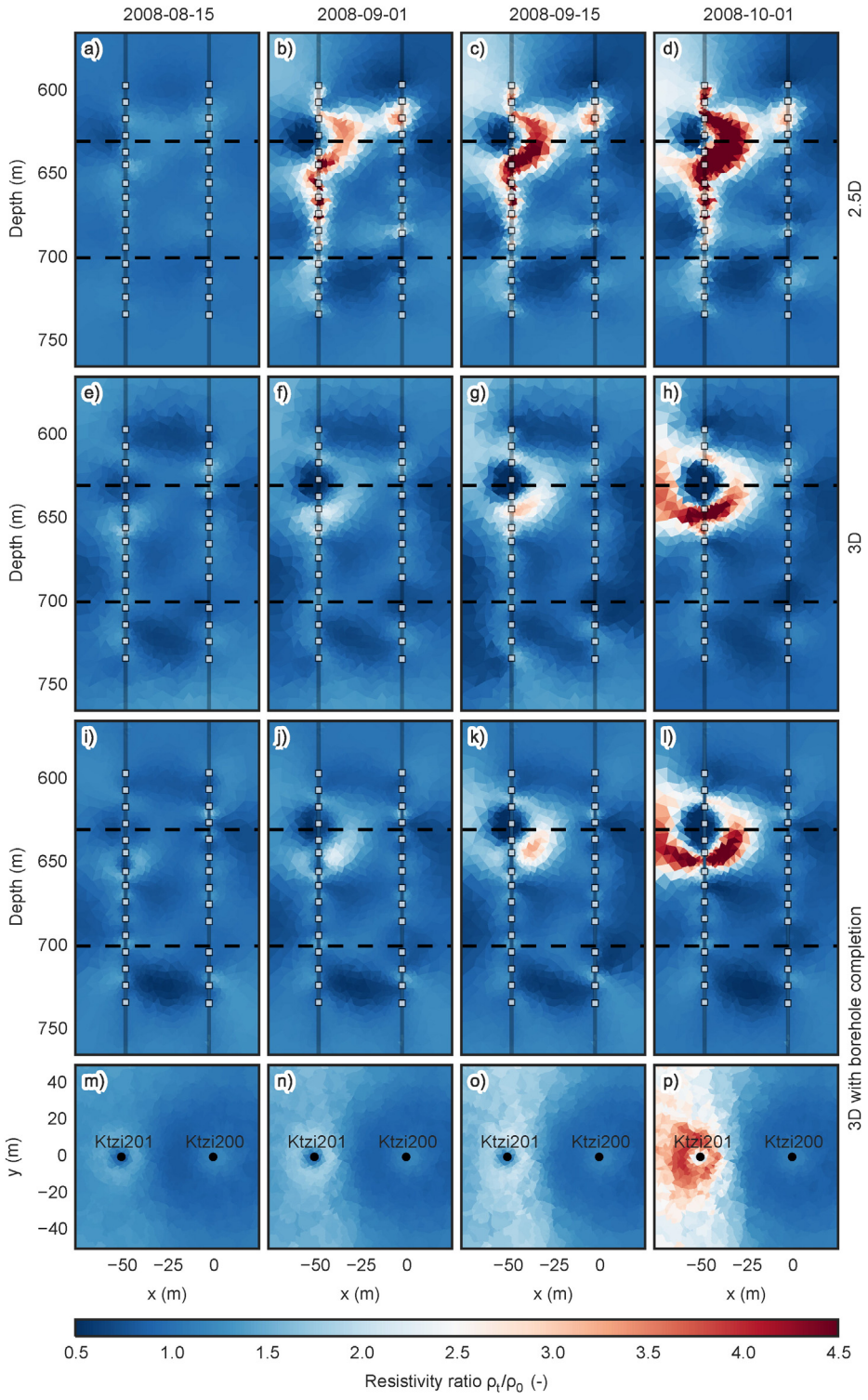

Fig. 9. Resistivity ratio of four consecutive timesteps with respect to baseline conditions using a 2.5D inversion (a–d), 3D inversion (e–h), and a borehole constrained inversion (i–l). The lower row (m–p) shows a depth slice through the resistive anomaly at $y = 650$ m of the borehole constrained inversion.

context of geophysical landslide monitoring, where the electrodes are naturally moving during data acquisition (Wilkinson et al., 2010, 2015; Kim et al., 2014). We adopt a similar approach here by expanding the model parameter vector with the x and z coordinates of the electrodes. To allow for a coupled inverse problem, the columns of the Jacobian matrix are expanded accordingly. In order to determine the sensitivity of electrode shifts on the measured data, we use a finite-difference approximation, i.e. each electrode position is shifted by 0.5 m in x and z directions and the forward problem is solved subsequently. The starting electrodes assume no borehole deviation and the nominal electrode spacing of 10 m. Remeshing during each iteration is not necessary since the present version of the forward operator based on Rücker et al. (2006) allows electrodes to be placed also within mesh cells. This ensures that the number of parameters remains constant throughout the inversion.

Kim et al. (2014) use three additional regularization terms acting on the electrode coordinates in the objective function and also discuss the difficulty of determining appropriate weights for each individual term.

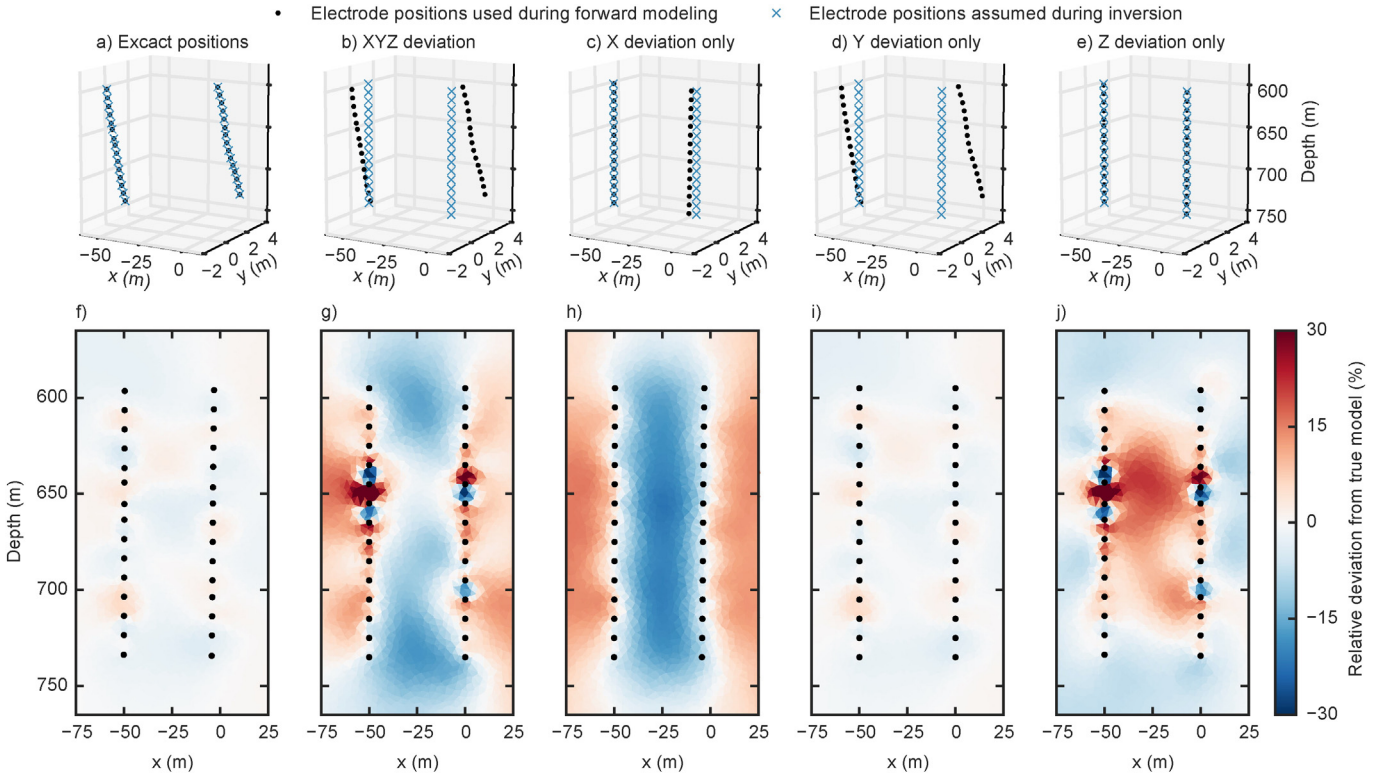

Fig. 10. Influence of 3D borehole deviation on tomographic inversion results of a homogeneous model. (a) Positions for forward modeling and inversion are the true, 3D deviated electrode positions. (b) Inversion assumes no borehole deviation. (c–e) Inversions assuming no borehole deviation when true positions are exclusively deviated in *x*, *y* and *z* directions, respectively. The lower row (f–j) shows the corresponding inversion results as slices through the 3D volumes at $y = 0$.

For the results in this paper, no additional regularization constraints are imposed, but linearity of the borehole trajectory segment in the reservoir is presumed to maintain stability of the inversion process. Hence, only the *x* coordinates of the upper and lower electrodes in each borehole are estimated during inversion, whereas the *x* coordinates of the electrodes in between are interpolated linearly. While the borehole trajectory over the entire borehole length may be arbitrarily curved, we assume that, due to the rigidity of the steel casing, a linear approximation is valid for the vertical distance of 140 m where the electrodes are located (e.g. Fig. 2c and d). In fact, the measured lateral deviations of the electrodes in this interval from a fitted straight line are within the centimeter range. No assumptions about the *z* coordinates are made, resulting in 34 additional unknowns for 30 electrodes.

5.2.1. Synthetic example

Fig. 11a shows a three layer resistivity model based on the averaged layer resistivities at the Ketzin site reported by Kiessling et al. (2010). Electrode positions used for the generation of synthetic data are marked by black circles. The depth coordinates of the electrodes correspond to the true coordinates of the electrodes at the Ketzin site. In addition, the right-hand borehole (representing Ktzi200) is tilted by 7.5 degrees. The data set used for the synthetic experiment comprises approximately 1000 four-point configurations that are regularly measured at the Ketzin site between wells Ktzi200 and Ktzi201 (Schmidt-Hattenberger et al., 2012). Prior to inversion, all data sets were contaminated with either 1% or 5% Gaussian noise.

Fig. 11b shows a conventional inversion result where the deviated electrode positions are assumed to be accurately known for a noise level of 1%. In comparison, Fig. 11c shows the result of a conventional inversion which ignores borehole deviations and assumes the nominal electrode spacing of 10 m. The subsurface resistivity is notably overestimated in regions where the electrodes are actually further apart than assumed during inversion, and vice versa. Pronounced near-electrode artifacts occur at electrodes with deviated *z* coordinates. This is in agreement with the analysis of borehole deviation effects presented in Fig. 10. Fig. 11d shows a result of the inversion when both the underlying resistivity distribution and the electrode locations are estimated jointly, hereinafter referred to as a coupled inversion. The coupled inversion outperforms the conventional one indicated by an enhanced reconstruction of the true layered resistivity model. In addition, estimated *x* and *z* coordinates (black dots) are in good agreement with the true electrode positions (black circles). It is important to note that all three inversion results shown in Fig. 11b–d have comparable data misfits, since electrodes misplacements are completely compensated by inversion artifacts in the conventional inversion with false electrode coordinates (Fig. 11c).

While generally promising, Fig. 11e–g demonstrates that the method is not robust for noise levels comparable to the Ketzin site, where the median reciprocal error ranges between 5% and 10% (Schmidt-Hattenberger et al., 2014). Here, the coupled inversion approach (Fig. 11g) shows similar spurious features as the conventional inversion (Fig. 11f). As a consequence, application of the coupled inversion to the Ketzin field data sets did not lead to stable inversion results.

6. Conclusions

Borehole-based electrical resistivity tomography is a powerful tool for CO_2 storage reservoir monitoring. When permanent electrodes are used, particular care should be taken with regard to the borehole environment. We specifically discussed the effects of the finite spatial extent of the ring electrodes, borehole completion, and borehole deviation. For the Ketzin site, a point representation is a valid approximation for the ring shaped electrodes, due to the relatively large electrode spacing of 10 m. When the electrode spacing is smaller or locally refined to increase the spatial resolution within the target horizon as suggested by Wagner et al. (2015), we recommend the use of the complete electrode model (Rücker and Günther, 2011).

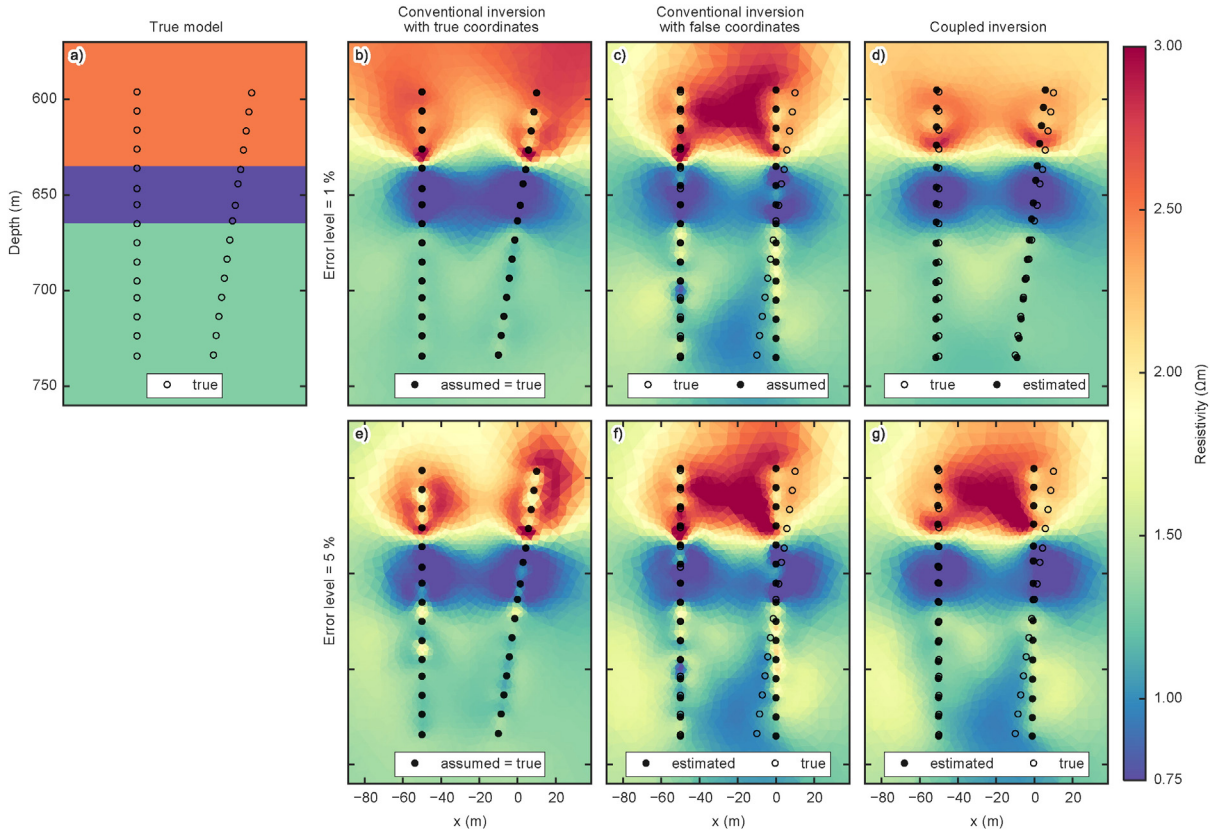

Fig. 11. (a) True resistivity model used for the generation of synthetic data. (b, e) Conventional inversion result using the exact electrode positions for 1% and 5% data noise, respectively. (c, f) Conventional inversion result assuming no borehole deviation and an equidistant electrode spacing of 10 m for 1% and 5% data noise, respectively. (d, g) Inversion result based on a simultaneous estimation of resistivities and electrode locations for 1% and 5% data noise, respectively.

Permanent crosshole ERT measurements are likely to be challenged by borehole completions. While the presence of completion materials that are more resistive than the rock formation play a minor role, care should be taken when the well annulus is filled with highly conductive fluids commonly encountered in deep storage formations, which is likely to favor current channeling. Doetsch et al. (2010) point out that the avoidance of measurement configurations with current injecting bipoles within one borehole is a possible mitigation strategy. Furthermore, an explicit discretization of the borehole completion into an unstructured finite-element mesh allows smoothness-constrained inversions to behave discontinuously across boundaries predefined by the borehole completion. This can result in tomograms better representing the subsurface conditions, which is particularly beneficial when an image of the absolute resistivity structure is desired compared to imaging relative changes (e.g. Nimmer et al., 2008; Doetsch et al., 2010). For the Ketzin case, a thinner and better confined CO_2 related resistivity anomaly is obtained by using 3D inversions instead of 2.5D inversions. We conclude that 3D inversions are more suitable to image injection processes, as they also allow for the imaging of confined circular resistivity anomalies. For the presented field study, the explicit incorporation of the different borehole completion materials does not show notable differences compared to conventional 3D inversions.

Additionally, attention should be paid to the potential occurrence of borehole deviations. Especially displacements of the electrodes along the z coordinate can introduce significant near-electrode artifacts in the tomographic images and should be accounted for in the inversions. Borehole deviations can potentially be estimated from the electrical data itself using a coupled inversion approach that simultaneously estimates the resistivity distribution and the electrode locations. In order to make coupled inversions more robust for field data sets with significant error components, further research with regard to the experimental design appears necessary. In particular, it would be beneficial to identify electrode configurations that are highly sensitive to geometric displacements (e.g. Wilkinson et al., 2008), while offering a robust signal to noise ratio for field applications.

Acknowledgments

We thank Dale Rucker and one anonymous reviewer for their constructive comments that have improved the clarity of the manuscript. Research funding is provided within Helmholtz-Alberta Initiative (HAI) by the Helmholtz Association's Initiative and Networking Fund, the participating Helmholtz Centers, and by the Government of Alberta through Alberta Environment's ecoTrust program. Jung-Ho Kim is gratefully acknowledged for the insights on estimating electrode positions from geoelectrical data.

References

Baumann, G., Henninges, J., DeLucia, M., 2014. Monitoring of saturation changes and salt precipitation during CO_2 injection using pulsed neutron-gamma logging at the Ketzin pilot site. Int. J. Greenh. Gas Control 28, 134–146. http://dx.doi.org/10.1016/j.ijggc.2014.06.023.

Bergmann, P., Schmidt-Hattenberger, C., Kiessling, D., Rücker, C., Labitzke, T., Henninges, J., Baumann, G., Schütt, H., 2012. Surface-downhole electrical resistivity tomography applied to monitoring of CO_2 storage at Ketzin, Germany. Geophysics 77, B253–B267. http://dx.doi.org/10.1190/geo2011-0515.1.

Binley, A., Kemna, A., 2005. DC resistivity and induced polarization methods. In: Rubin, Y., Hubbard, S. (Eds.), Hydrogeophysics vol. 50. Springer Netherlands, pp. 129–156. http://dx.doi.org/10.1007/1-4020-3102-5_5.

Carrigan, C., Yang, X., LaBrecque, D.J., Larsen, D., Freeman, D., Ramirez, A.L., Daily, W., Aines, R., Newmark, R., Friedmann, J., Hovorka, S., 2013. Electrical resistance tomographic monitoring of CO_2 movement in deep geologic reservoirs. Int. J. Greenh. Gas Control 18, 401–408. http://dx.doi.org/10.1016/j.ijggc.2013.04.016.

Doetsch, J.A., Coscia, I., Greenhalgh, S., Linde, N., Green, A.G., Günther, T., 2010. The borehole-fluid effect in electrical resistivity imaging. Geophysics 75, F107–F114. http://dx.doi.org/10.1190/1.3467824.

Förster, A., Norden, B., Zinck-Jørgensen, K., Frykman, P., Kulenkampff, J., Spangenberg, E., Erzinger, J., Zimmer, M., Kopp, J., Borm, G., Juhlin, C., Cosma, C.G., Hurter, S., 2006. Baseline characterization of the CO_2SINK geological storage site at Ketzin, Germany. Environ. Geosci. 13, 145–161. http://dx.doi.org/10.1306/eg.02080605016.

Friedel, S., 2003. Resolution, stability and efficiency of resistivity tomography estimated from a generalized inverse approach. Geophys. J. Int. 153, 305–316. http://dx.doi.org/10.1046/j.1365-246X.2003.01890.x.

Götz, J., 2013. Borehole seismic monitoring of CO_2 storage within a saline aquifer at Ketzin, Germany (Ph.D. thesis) Technische Universität Berlin.

Hagrey, S., Kohn, D., Wiegers, C., D., S., Rabbel, W., 2014. Feasibility study for geophysical monitoring renewable gas energy compressed in pore storages. J. Geol. Geosci. 3, 1–9. http://dx.doi.org/10.4172/2329-6755.1000169.

Kiessling, D., Schmidt-Hattenberger, C., Schütt, H., Schilling, F.R., Krüger, K., Schöbel, B., Danckwardt, E., Kummerow, J., 2010. Geoelectrical methods for monitoring geological CO_2 storage: first results from cross-hole and surface-downhole measurements from the CO_2SINK test site at Ketzin (Germany). Int. J. Greenh. Gas Control 4, 816–826. http://dx.doi.org/10.1016/j.ijggc.2010.05.001.

Kim, J., Yi, M., Supper, R., Ottowitz, D., 2014. Simultaneous inversion of resistivity structure and electrode locations in ERT. Near Surface Geoscience 2014 — 20th European Meeting of Environmental and Engineering Geophysics. EAGE Publications BV http://dx.doi.org/10.3997/2214–4609.20142057.

Köhler, S., Zemke, J., Becker, W., Wiebach, J., Liebscher, A., Möller, F., Bannach, A., 2013. Operational reservoir monitoring at the CO_2 pilot storage site Ketzin, Germany. In: Hou, M.Z., Xie, H., Were, P. (Eds.), Clean Energy Systems in the Subsurface: Production, Storage and ConversionSpringer Series in Geomechanics and Geoengineering. Springer Berlin Heidelberg, pp. 53–63. http://dx.doi.org/10.1007/978-3-642-37849-2_5.

Kühn, M., Liebscher, A., Martens, S., Möller, F., Kempka, T., Streibel, M., 2015. Safe operation of geological CO_2 storage using the example of the pilot site in Ketzin. Carbon Capture, Storage and Use. Springer International Publishing, pp. 127–143. http://dx.doi.org/10.1007/978–3-319-11943-4_6.

Loke, M., Chambers, J., Rucker, D., Kuras, O., Wilkinson, P., 2013. Recent developments in the direct-current geoelectrical imaging method. J. Appl. Geophys. 95, 135–156. http://dx.doi.org/10.1016/j.jappgeo.2013.02.017.

Martens, S., Möller, F., Streibel, M., Liebscher, A., 2014. Completion of five years of safe CO_2 injection and transition to the post-closure phase at the Ketzin pilot site. Energy Procedia 59, 190–197. http://dx.doi.org/10.1016/j.egypro.2014.10.366.

Maurer, H.R., 1996. Systematic errors in seismic crosshole data: application of the coupled inverse technique. Geophys. Res. Lett. 23, 2681–2684. http://dx.doi.org/10.1029/96gl02068.

Maurer, H., Musil, M., 2004. Effects and removal of systematic errors in crosshole georadar attenuation tomography. J. Appl. Geophys. 55, 261–270. http://dx.doi.org/10.1016/j.jappgeo.2004.02.003.

Nimmer, R.E., Osiensky, J.L., Binley, A.M., Williams, B.C., 2008. Three-dimensional effects causing artifacts in two-dimensional, cross-borehole, electrical imaging. J. Hydrol. 359, 59–70. http://dx.doi.org/10.1016/j.jhydrol.2008.06.022.

Norden, B., Frykman, P., 2013. Geological modelling of the triassic stuttgart formation at the Ketzin CO_2 storage site, Germany. Int. J. Greenh. Gas Control 19, 756–774. http://dx.doi.org/10.1016/j.ijggc.2013.04.019.

Oldenborger, G.A., Routh, P.S., Knoll, M.D., 2005. Sensitivity of electrical resistivity tomography data to electrode position errors. Geophys. J. Int. 163, 1–9. http://dx.doi.org/10.1111/j.1365-246X.2005.02714.x.

Osiensky, J.L., Nimmer, R., Binley, A.M., 2004. Borehole cylindrical noise during hole-surface and hole–hole resistivity measurements. J. Hydrol. 289, 78–94. http://dx.doi.org/10.1016/j.jhydrol.2003.11.003.

Prevedel, B., Wohlgemuth, L., Henninges, J., Krüger, K., Norden, B., Förster, A., 2008. The CO_2SINK boreholes for geological storage testing. Sci. Drill. http://dx.doi.org/10.2204/iodp.sd.6.04.2008.

Rücker, C., Günther, T., 2011. The simulation of finite ERT electrodes using the complete electrode model. Geophysics 76, F227–F238. http://dx.doi.org/10.1190/1.3581356.

Rücker, C., Günther, T., Spitzer, K., 2006. Three-dimensional modelling and inversion of dc resistivity data incorporating topography — I. Modelling. Geophys. J. Int. 166, 495–505. http://dx.doi.org/10.1111/j.1365-246X.2006.03010.x.

Schmidt-Hattenberger, C., Bergmann, P., Bösing, D., Labitzke, T., Möller, M., Schröder, S., Wagner, F., Schütt, H., 2013. Electrical resistivity tomography (ERT) for monitoring of CO_2 migration — from tool development to reservoir surveillance at the Ketzin pilot site. Energy Procedia 37, 4268–4275. http://dx.doi.org/10.1016/j.egypro.2013.06.329.

Schmidt-Hattenberger, C., Bergmann, P., Kießling, D., Krüger, K., Rücker, C., Schütt, H., 2011. Application of a vertical electrical resistivity array (VERA) for monitoring CO_2 migration at the ketzin site: first performance evaluation. Energy Procedia 4, 3363–3370. http://dx.doi.org/10.1016/j.egypro.2011.02.258.

Schmidt-Hattenberger, C., Bergmann, P., Labitzke, T., Schröder, S., Krüger, K., Rücker, C., Schütt, H., 2012. A modular geoelectrical monitoring system as part of the surveillance concept in CO_2 storage projects. Energy Procedia 23, 400–407. http://dx.doi.org/10.1016/j.egypro.2012.06.062.

Schmidt-Hattenberger, C., Bergmann, P., Labitzke, T., Wagner, F., 2014. CO_2 migration monitoring by means of electrical resistivity tomography (ERT) — review on five years of operation of a permanent ERT system at the ketzin pilot site. Energy Procedia 63, 4366–4373. http://dx.doi.org/10.1016/j.egypro.2014.11.471.

Soleimani, M., Gómez-Laberge, C., Adler, A., 2006. Imaging of conductivity changes and electrode movement in EIT. Physiol. Meas. 27, S103–S113. http://dx.doi.org/10.1088/0967-3334/27/5/s09.

Tøndel, R., Schütt, H., Dümmong, S., Ducrocq, A., Godfrey, R., LaBrecque, D., Nutt, L., Campbell, A., Rufino, R., 2014. Reservoir monitoring of steam-assisted gravity drainage using borehole measurements. Geophys. Prospect. 62, 760–778. http://dx.doi.org/10.1111/1365-2478.12131.

Vilamajó, E., Queralt, P., Ledo, J., Marcuello, A., 2013. Feasibility of monitoring the hontomín (Burgos, Spain) CO_2 storage site using a deep EM source. Surv. Geophys. 34, 441–461. http://dx.doi.org/10.1007/s10712-013-9238-y.

Wagner, F., Günther, T., Schmidt-Hattenberger, C., Maurer, H., 2015. Constructive optimization of electrode locations for target-focused resistivity monitoring. Geophysics 80, E29–E40. http://dx.doi.org/10.1190/geo2014-0214.1.

Wilkinson, P.B., Chambers, J.E., Lelliott, M., Wealthall, G.P., Ogilvy, R.D., 2008. Extreme sensitivity of crosshole electrical resistivity tomography measurements to geometric errors. Geophys. J. Int. 173, 49–62. http://dx.doi.org/10.1111/j.1365-246X.2008.03725.x.

Wilkinson, P.B., Chambers, J.E., Meldrum, P.I., Gunn, D.A., Ogilvy, R.D., Kuras, O., 2010. Predicting the movements of permanently installed electrodes on an active landslide using time-lapse geoelectrical resistivity data only. Geophys. J. Int. 183, 543–556. http://dx.doi.org/10.1111/j.1365-246X.2010.04760.x.

Wilkinson, P.B., Uhlemann, S.S., Chambers, J.E., Meldrum, P.I., Loke, M.H., 2015. Development and testing of displacement inversion to track electrode movements on 3-D electrical resistivity tomography monitoring grids. Geophys. J. Int. 200, 1566–1581. http://dx.doi.org/10.1093/gji/ggu483.

Yang, X., Chen, X., Carrigan, C.R., Ramirez, A.L., 2014. Uncertainty quantification of CO_2 saturation estimated from electrical resistance tomography data at the Cranfield site. Int. J. Greenh. Gas Control 27, 59–68. http://dx.doi.org/10.1016/j.ijggc.2014.05.006.

Yi, M.J., Kim, J.H., Son, J.S., 2009. Borehole deviation effect in electrical resistivity tomography. Geosci. J. 13, 87–102. http://dx.doi.org/10.1007/s12303-009-0008-2.